Direct Evidence for the vd512 Orbital in 69Ni: Implications for the N=40 Island of Inversion

Downloaded from: https://research.chalmers.se, 2026-01-21 18:20 UTC

Citation for the original published paper (version of record):

Ceulemans, A., Raabe, R., Nowacki, F. et al (2025). Direct Evidence for the vd512 Orbital in 69Ni: Implications for the N=40 Island of Inversion. Physical Review Letters, 135(25). http://dx.doi.org/10.1103/tdfs-5qzw

N.B. When citing this work, cite the original published paper.

research.chalmers.se offers the possibility of retrieving research publications produced at Chalmers University of Technology. It covers all kind of research output: articles, dissertations, conference papers, reports etc. since 2004. research.chalmers.se is administrated and maintained by Chalmers Library

(article starts on next page)

Direct Evidence for the $\nu d_{5/2}$ Orbital in ^{69}Ni: Implications for the $N = 40$ Island of Inversion

A. Ceulemans,[1,*] R. Raabe,[1,†] F. Nowacki,[2] A. Alharbi,[3,4] H. Ayatollahzadeh,[5,6] S. A. Bennett,[7] F. Browne,[8] P. A. Butler,[3] A. Camaiani,[1,‡] D. Clarke,[7] A. J. Dolan,[3] Z. Eleme,[9] C. T. A. Everett,[3] F. Flavigny,[10] S. Fracassetti,[1] S. J. Freeman,[7,8] L. P. Gaffney,[3] G. Georgiev,[8,11] S. Goula,[9] A. Heinz,[12] A. Kawęcka,[12] J. M. Keatings,[5,6] M. Labiche,[13] I. Lazarus,[13] P. T. MacGregor,[7,8] M. V. Managlia,[12] J. Ojala,[3,§] B. Olaizola,[8,‖] R. D. Page,[3] N. Patronis,[9] O. Poleshchuk,[1] A. M. Sánchez-Benítez,[14] D. K. Sharp,[7] H. Törnqvist,[12] and A. Youssef[1]

(ISS Collaboration)
(ISOLDE Collaboration)

[1]*Instituut voor Kern- en Stralingsfysica, KU Leuven, Leuven 3001, Belgium*
[2]*Université de Strasbourg, CNRS, IPHC UMR 7178, 23 rue du Loess, F-67000 Strasbourg, France*
[3]*Department of Physics, University of Liverpool, Liverpool L69 7ZE, United Kingdom*
[4]*Physics Department, College of Science, Qassim University, Buraydah 51452, Saudi Arabia*
[5]*School of Computing, Engineering, and Physical Sciences, University of the West of Scotland, Paisley PA1 2BE, United Kingdom*
[6]*SUPA, Scottish Universities Physics Alliance, Glasgow, G12 8QQ United Kingdom*
[7]*Department of Physics and Astronomy, University of Manchester, Manchester M13 9PL, United Kingdom*
[8]*CERN, Geneva 23 CH-1211, Switzerland*
[9]*Department of Physics, University of Ioannina, Ioannina 45110, Greece*
[10]*LPC Caen, Normandie Université, ENSICAEN, UNICAEN, CNRS/IN2P3, Caen 14000, France*
[11]*IJCLab, CNRS/IN2P3, Université Paris-Saclay, F-91405 Orsay, France*
[12]*Department of Physics, Chalmers University of Technology, Göteborg 412 96, Sweden*
[13]*Nuclear Physics Group, UKRI-STFC Daresbury Laboratory, Daresbury, Warrington WA4 4AD, United Kingdom*
[14]*Department of Integrated Sciences, Centro de Estudios Avanzados en Fisica, Matematicas y Computacion (CEAFMC), University of Huelva, Huelva 21071, Spain*

(Received 17 June 2025; revised 11 September 2025; accepted 12 November 2025; published 19 December 2025)

Shape coexistence, a collective manifestation of nuclear structure, emerges from the underlying single-particle dynamics and is prominently observed in the region below ^{68}Ni. Theoretical studies have emphasized the key role of the $\nu d_{5/2}$ orbital, the quadrupole partner of $\nu g_{9/2}$, in driving deformation. However, experimental constraints on the location and properties of neutron orbitals in neutron-rich isotopes in this region remain scarce. In this Letter, the single-particle structure of ^{69}Ni was investigated via the ^{68}Ni(d, p) reaction in inverse kinematics, performed at the ISOLDE Solenoidal Spectrometer at CERN. Several new excited states were observed, and comparisons with adiabatic distorted wave approximation (ADWA) calculations enabled ℓ-value assignments for the most strongly populated states. In particular, a state at 2.56 MeV is interpreted as the dominant fragment of the $\nu d_{5/2}$ strength. The experimental findings are well reproduced by Large-Scale Shell Model calculations using a modified LNPS interaction with an increased $\nu g_{9/2}$–$\nu d_{5/2}$ energy gap. These results provide new insight into the structure of ^{69}Ni and underscore the crucial role of the $\nu d_{5/2}$ orbital in the onset of collectivity at the $N = 40$ island of inversion.

DOI: 10.1103/tdfs-5qzw

*Contact author: andreas.ceulemans@kuleuven.be
†Contact author: riccardo.raabe@kuleuven.be
‡Present address: Dipartimento di Fisica, Università degli Studi di Firenze e INFN-Firenze, Firenze, 50019, Italy.
§Present address: Accelerator Laboratory, Department of Physics, University of Jyväskylä, FI-40014 Jyväskylä, Finland.
‖Present address: Instituto de Estructura de la Materia, CSIC, 28006 Madrid, Spain.

Published by the American Physical Society under the terms of the Creative Commons Attribution 4.0 International license. Further distribution of this work must maintain attribution to the author(s) and the published article's title, journal citation, and DOI. Open access publication funded by CERN.

The phenomenon of shape coexistence has emerged as a hallmark of nuclear structure, reflecting the intricate interplay between single-particle motion and collective dynamics [1]. It manifests as the presence of multiple configurations with distinct intrinsic deformations at low excitation energies, often within the same nucleus. These configurations arise from the competition between mean-field shapes, shell effects, and residual interactions, playing a central role in the evolution of nuclear structure across the chart of nuclides. Clarifying the connection between shape coexistence and single-particle degrees of freedom remains a central challenge for modern theoretical approaches [2].

Prominent examples occur in neutron-deficient nuclei near $Z = 82$. In ^{186}Pb, the ground and two lowest excited states are all 0^+ states with differing shapes [3,4], while shape staggering is observed in the ground states of Hg isotopes between $A = 177$ and $A = 181$ [5]. In this region, elucidating the role of specific orbitals is both experimentally and theoretically demanding. Only recently have Monte Carlo shell model calculations provided insight into the structure of the Hg isotopes [5].

In lighter nuclei, where large-scale shell model calculations are tractable, the connection between collective and single-particle phenomena is more clearly established. The well-known island of inversion near ^{32}Mg exemplifies shape coexistence [6–11], where the conventional $N = 20$ magic number is quenched, enabling neutrons to occupy fp orbitals across a reduced energy gap [12]. Quadrupole correlations favor deformed two-particle–two-hole configurations [13]. Similarly, measurements of 2^+ states in $N = 28$ isotones [14,15] indicate a weakening of the $N = 28$ shell gap from ^{48}Ca to ^{42}Si. Theoretical studies predict shape coexistence in ^{44}S and deformed ground states in ^{42}Si and ^{40}Mg [16,17].

Another region of enhanced collectivity arises at $N = 40$, below the $Z = 28$ nucleus ^{68}Ni. Although the $N = 40$ harmonic oscillator shell closure might suggest a doubly magic character for ^{68}Ni, experimental evidence remains inconclusive [18–23]. The observation of several low-lying 0^+ states in this nucleus [18,24,25] suggests shape coexistence [26–28], associated with the Quasi-SU(3) sequence involving the $g_{9/2}$, $d_{5/2}$, and $s_{1/2}$ orbitals above $N = 40$ [29]. With proton removal, the tensor force reduces the $N = 40$ shell gap, favoring deformed intruder ground states in ^{66}Fe and ^{62}Cr [30], thereby establishing a new island of inversion. Maximum collectivity is observed in ^{64}Cr [31], and recent investigations suggest that ^{62}Ti also belongs to this island [32].

Large-scale shell model (LSSM) calculations using the LNPS interaction [29,33] allow for neutron excitations across $N = 40$, yielding a comprehensive description of nuclear structure phenomena in this region. These descriptions include the spectroscopy in the region of neutron-rich calcium isotopes [29,32,34], the coexistence of normal and intruder configurations in the vicinity of ^{68}Ni [26,35,36], and the emergence of collectivity leading to the $N = 40$ island of inversion [30,33,37–39]. For ^{60}Ca, the LNPS interaction predicts a vanishing $N = 40$ shell gap and near degeneracy of the $g_{9/2}$ and $d_{5/2}$ neutron orbitals. This results in exotic properties, including a deformed ground state with more than three neutrons promoted above $N = 40$, and a rotational-like spectrum distorted by pairing correlations [29].

Although ^{60}Ca lies beyond current experimental reach, mapping the evolution of the $g_{9/2}$ and $d_{5/2}$ orbitals in this region remains essential, as their relative energies are critical to the onset of collectivity below ^{68}Ni.

Direct reactions are a powerful tool for probing single-particle structure. Their selectivity enables the extraction of spectroscopic factors and angular momentum assignments. In nuclei up to $N = 40$ that are experimentally accessible, neutron-adding reactions such as (d, p) provide access to the $g_{9/2}$ and $d_{5/2}$ orbitals, offering a direct means to investigate the microscopic mechanisms underlying shape coexistence and deformation.

In this Letter, we report a new measurement of the ^{68}Ni$(d, p)^{69}$Ni reaction in inverse kinematics at a beam energy of 6 MeV/nucleon. A previous study of this reaction [40,41] observed partial $d_{5/2}$ strength; however, limited resolution precluded firm spin-parity assignments. The improved resolution of the present measurement enabled the identification of several low-lying states in ^{69}Ni, along with definitive spin-parity assignments for the most strongly populated levels. The $g_{9/2}$ strength is confirmed to be concentrated in the ground state, while a state at 2.56 MeV is strongly populated via $\ell = 2$ transfer and is interpreted as the dominant fragment of the $d_{5/2}$ strength. Comparison with LSSM calculations provides a new estimate of the energy gap between the $\nu g_{9/2}$ and $\nu d_{5/2}$ orbitals, with implications for the structure of neutron-rich nuclei in the $N = 40$ island of inversion.

The experiment was conducted at the ISOLDE facility at CERN using a radioactive ^{68}Ni ion beam, produced by bombarding a uranium carbide target with 1.4 GeV protons from the PS Booster. Selective ionization of nickel atoms was achieved via the Resonance Ionization Laser Ion Source (RILIS) [42]. Mass separation with the ISOLDE General Purpose Separator removed nonisobaric contaminants, and the resulting ^{68}Ni ions were accumulated and cooled in REXTRAP before being injected into REXEBIS. There, they were charge bred to $q = 18^+$ and accelerated to 6 MeV/nucleon using the HIE-ISOLDE postaccelerator [43]. A 137-μg/cm^2 deuterated-polyethylene (CD_2) target induced the (d, p) reaction. A background contribution from ^{68}Ga, which is surface ionized, was characterized by acquiring laser-off data to enable background subtraction.

Reaction products were detected using the ISOLDE Solenoidal Spectrometer (ISS) [44], a setup optimized for two-body reactions in inverse kinematics. A uniform magnetic field ($B = 2.05$ T) aligned with the beam axis

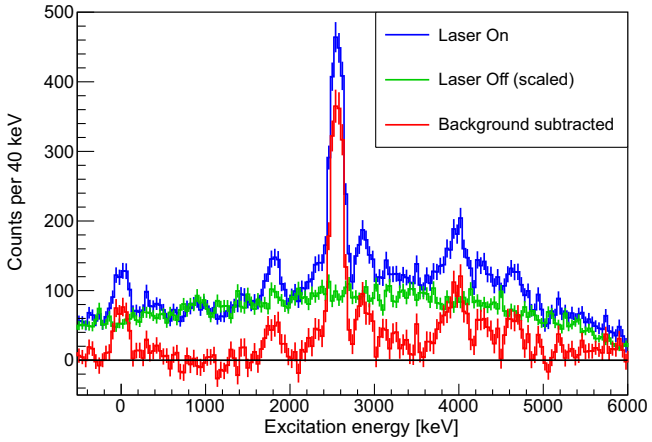

FIG. 1. Detected protons as a function of the calculated excitation energy in ^{69}Ni. Data acquired with lasers on (containing both Ni- and Ga-induced events) are shown in blue. The Ga-only background (lasers off) is shown in green and scaled to match the background region. The background-subtracted spectrum is shown in red.

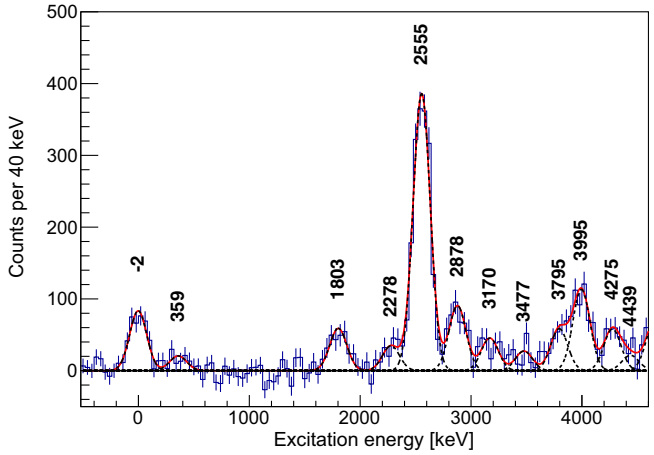

FIG. 2. Background-subtracted excitation-energy spectrum of ^{69}Ni populated in the ^{68}Ni(d,p) reaction, up to the neutron separation energy at 4586 keV [49]. Peaks were fitted with Gaussian functions; excitation energies (in keV) are indicated above each peak.

caused light reaction products to execute a single cyclotron orbit, focusing them back to the axis where they were detected with a position-sensitive silicon array. This geometry improves the excitation-energy resolution of the inverse-kinematics (d,p) measurement [45]. Protons were detected at backward laboratory angles, corresponding to forward center-of-mass angles where the (d,p) cross section is largest and contamination from elastic and $(d,{}^3\mathrm{He})$ channels is minimized.

Absolute normalization of the differential cross sections was performed using elastically scattered deuterons detected at forward angles in an annular silicon detector. Data analysis was carried out using the ISSSort software package [46] and the ROOT framework [47]. Excitation energies and center-of-mass angles were reconstructed from the measured proton energies and positions following the method of Ref. [45].

Figure 1 shows the number of detected protons in the silicon array as a function of the calculated excitation energy in ^{69}Ni. A contaminant ^{68}Ga component in the beam contributes background events, isolated via laser-off data which contain only Ga-induced reactions. This spectrum was scaled to match the laser-on data in the region from -2000 to -500 keV, where no true ^{69}Ni states are expected, and subtracted to yield the background-corrected excitation spectrum. The resulting peaks were fitted with Gaussian functions using a fixed width of 181 keV (FWHM), determined from the strongest observed transition. The fitted spectrum is presented in Fig. 2. Simulations were performed using the NPTOOL framework [48] to determine the geometric efficiency of the detector and to evaluate systematic uncertainties as a function of excitation energy. These included contributions from the beam energy, target position and thickness, magnetic field strength, and detector dead layer. The nominal target position used by the sorting software was adjusted such that the reconstructed ground-state peak lies at 0 keV. Uncertainties for all identified levels are summarized in Table I.

TABLE I. Excitation energy E_x, transferred angular momentum ℓ, assigned spin-parity J^π, and spectroscopic factor S for states in ^{69}Ni populated in the ^{68}Ni(d,p) reaction. The first uncertainty on E_x is statistical (from the peak fit); the value in parentheses reflects the systematic uncertainty derived from simulations. Tentative assignments of J^π, ℓ, and S are indicated in parentheses. For states where no values are given the assignment was inconclusive. Spectroscopic factors were extracted via comparison with ADWA calculations using the optical-model parameters of Koning and Delaroche [50], and normalized using elastic cross sections calculated with the parameters of Daehnick *et al.* [51]. Quoted uncertainties on S include statistical and systematic components (in parentheses). States above the neutron-separation energy are not listed.

E_x (keV)	ℓ	J^π	S
$-2 \pm 10^{[+0]}_{[-0]}$	4	$9/2^+$	$0.99 \pm 0.09^{[+1.15]}_{[-0.18]}$
$359 \pm 47^{[+2]}_{[-1]}$	1	$1/2^-$	$0.11 \pm 0.03^{[+0.12]}_{[-0.02]}$
$1803 \pm 16^{[+10]}_{[-4]}$	2	$5/2^+$	$0.08 \pm 0.01^{[+0.09]}_{[-0.01]}$
$2278 \pm 21^{[+14]}_{[-6]}$			
$2555 \pm 3^{[+15]}_{[-7]}$	2	$5/2^+$	$0.48 \pm 0.02^{[+0.55]}_{[-0.09]}$
$2878 \pm 13^{[+17]}_{[-8]}$			
$3170 \pm 28^{[+19]}_{[-8]}$			
$3477 \pm 32^{[+21]}_{[-10]}$			
$3795 \pm 24^{[+22]}_{[-11]}$	(0)	$(1/2^+)$	$(0.67 \pm 0.09^{[+0.77]}_{[-0.12]})$
$3995 \pm 12^{[+23]}_{[-11]}$			
$4275 \pm 26^{[+25]}_{[-13]}$	(1 or 2)		
$4439 \pm 77^{[+27]}_{[-14]}$			

Experimental angular distributions were obtained by normalizing the yield to the detector solid angle and the normalization factor from elastic scattering. Angular distributions for the most prominent states are shown in Fig. 3.

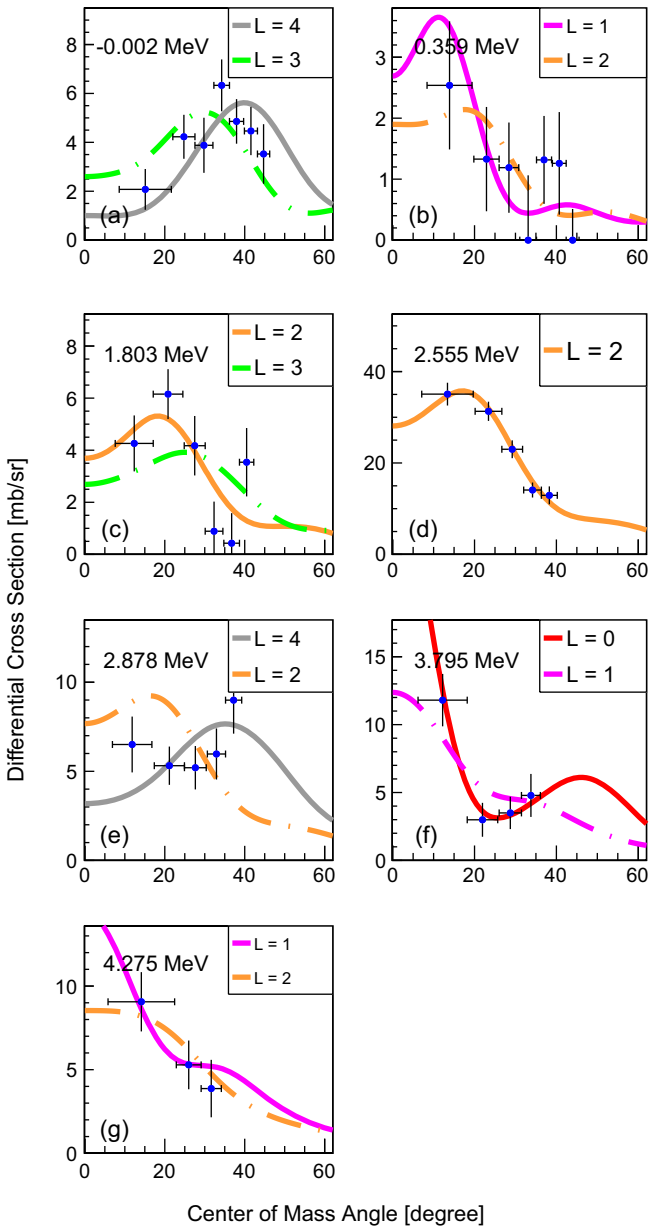

FIG. 3. Experimental differential cross sections (points with error bars) compared to ADWA calculations (solid and dashed lines) for states with a (tentative) spin assignment in ^{69}Ni. The solid lines correspond to the most likely angular momentum transfer ℓ, while dashed lines indicate alternative assignments. Horizontal error bars denote the angular coverage of each data point, and vertical bars represent statistical uncertainties. Data points correspond to center-of-mass angular bins derived from detector segments along the beam axis. The varying angular resolution across the distribution reflects the geometry of the detection setup.

Horizontal error bars reflect the angular range covered by each detector segment, while vertical bars denote statistical uncertainties.

Adiabatic distorted wave approximation (ADWA) calculations were performed using the code FRESCO [52] to evaluate theoretical angular distributions and cross sections. The adiabatic potentials were generated with the FRONT module of the TWOFNR package [53].

Calculations considered values of the transferred angular momentum ℓ from 0 to 4, consistent with the available orbitals in this mass region. Optical-model parameters were taken from Ref. [50]. Binding potentials for the $^{68}\mathrm{Ni}+n$ and $p+n$ systems were of Woods-Saxon form, comprising a real central and a spin-orbit term, using parameters from Refs. [54,55]. The real potential depth was adjusted to reproduce the neutron separation energy, while the spin-orbit depth was fixed at $V_{\mathrm{so}}=6$ MeV. Radius and diffuseness parameters were $r_0=1.28$ fm, $r_{\mathrm{so}}=1.10$ fm, and $a_0=a_{\mathrm{so}}=0.65$ fm. The outgoing wave potential was identical to the core-core potential. Input files used for these calculations are available in the code repository for this experiment [56].

The resulting calculated angular distributions are compared to the data in Fig. 3. Assignments of ℓ were made based on the position of the first maximum in the angular distribution, the quality of the fit, and the resulting spectroscopic factor. The most likely ℓ transfer is indicated by solid lines; when comparable in quality, the second best fit is indicated by dashed lines.

Two states were assigned to $\ell=2$, the most intense peak at 2.56 MeV and a smaller peak at 1.80 MeV. A state at 1.82 MeV, previously reported in Ref. [57], was interpreted as a $7/2^-$ level arising from an excited ^{68}Ni core. In the present measurement, such a configuration could only be populated via a two-step process, which is inconsistent with the strong yield observed. Additionally, a direct $\ell=3$ transfer to the nearly filled $f_{5/2}$ orbital is unlikely [26]. We therefore assign spin-parity $5/2^+$ to the 1.80 MeV state. The 2.56 MeV state shows a clear $\ell=2$ angular distribution and is also assigned $J^\pi=5/2^+$. This state accounts for the majority of the observed $\nu d_{5/2}$ strength [Fig. 3(d)]. In the previous measurement [41], the peak observed at 2.48 MeV was interpreted as two states at 2.05 and 2.74 MeV, both possibly $\ell=2$, with the latter also compatible with $\ell=4$. The improved energy resolution in the present Letter (181 keV FWHM vs ~1 MeV in Ref. [41]) resolves this structure into at least five distinct states.

The ground state [Fig. 3(a)], previously assigned $J^\pi=9/2^+$ [41,58], is compatible with both $\ell=3$ and $\ell=4$ in our analysis. However, the large extracted spectroscopic factor for $\ell=3$ is inconsistent with the near-full occupancy of the $\nu f_{5/2}$ orbital [26], favoring an $\ell=4$ assignment. A peak at 359 keV is consistent with the $J^\pi=1/2^-$ state at 321 keV observed in decay studies [57,59,60]. Its

TABLE II. Comparison between experimental and LNPS results (for both LNPS and LNPS† models) for states in ^{69}Ni involving the $\nu 1g_{9/2}$ and $\nu 2d_{5/2}$ orbitals. Listed are the excitation energy E_x, transferred angular momentum ℓ, assigned spin-parity J^{π}, and spectroscopic factor S. Dominant configurations are shown in bold. See Table I for uncertainties on the experimental results.

Experimental				LNPS				**LNPS†**			
E_x (keV)	ℓ	J^{π}	S	E_x (keV)	ℓ	J^{π}	S	E_x (keV)	ℓ	J^{π}	S
−2	**4**	**$9/2^+$**	**0.99**	**0**	**4**	**$9/2^+$**	**0.883**	**0**	**4**	**$9/2^+$**	**0.88**
1803	**2**	**$5/2^+$**	**0.08**	1695	2	$5/2^+$	0.010	1768	4	$5/2^+$	3.3×10^{-3}
2555	**2**	**$5/2^+$**	**0.48**	**2005**	**2**	$5/2^+$	**0.461**	**2190**	**2**	**$5/2^+$**	**0.19**
				2400	**2**	**$5/2^+$**	**0.387**	**2695**	**2**	**$5/2^+$**	**0.49**
				2722	2	$5/2^+$	0.032	**2893**	**2**	**$5/2^+$**	**0.18**

prominence at forward center-of-mass angles [Fig. 3(b)] supports a low-ℓ assignment, with $\ell = 1$ preferred. The weak population is expected due to the significant occupancy of the $p_{1/2}$ orbital in the ^{68}Ni ground state [26]. Additional states were observed, including some above the neutron-separation energy ($S_n = 4586$ keV [49]).

Spectroscopic factors (S in Table I) were extracted as ratios of the ADWA calculations to the experimental cross sections. Statistical uncertainties stem from experimental yields and range from ∼4% (most intense peak) to ∼27% (359 keV state). Systematic uncertainties arise from both experimental normalization and model assumptions. For the former, the normalization to elastic scattering and the target-detector distance contribute ∼3% uncertainty across all states. To assess model dependence, eight optical-model parametrizations for the (d,p) reaction and three for the (d,d) elastic scattering were considered, yielding deviations on the spectroscopic factors between around −10% and +50%, and 0% and +20%, respectively. Following Ref. [61], variations of the bound-state central and spin-orbit potential radii were also explored: r_c from 1.15 to 1.30 fm and r_{so} from 1.00 to 1.20 fm, leading to deviations of about −10% to +100% and −10% to +10%, respectively. We therefore estimate total systematic uncertainties on the spectroscopic factors to range from around −20% to +120%.

Despite the large systematic uncertainties, the spectroscopic factors show a good consistency within each modelization of the reaction. This allows a discussion of the strength distribution and the gap between the $\nu g_{9/2}$ and $\nu d_{5/2}$ orbitals.

The discussion is based on the comparison between our results and the prediction of Large-Scale Shell Model (LSSM) calculations based on the LNPS interaction [29,33].

The LSSM calculations comprise a ^{48}Ca core and a valence space consisting of the pf shell for protons and five orbitals for neutrons: $\nu 2p_{3/2}$, $\nu 1f_{5/2}$, $\nu 2p_{1/2}$, $\nu 1g_{9/2}$, and $\nu 2d_{5/2}$.

The inclusion of the $g_{9/2}$ and $d_{5/2}$ intruder orbitals allows breaking the $N = 40$ core and forming a Quasi-SU3 block which drives quadrupole correlations [62,63]. A key feature is the evolution of the splitting of the energy centroids $\langle g_{9/2}\rangle$–$\langle d_{5/2}\rangle$ with proton number along $N = 40$, which must remain sufficiently small to induce deformation in the island of inversion but large enough to preserve the spherical character in nickel isotopes. Current estimates show near-degeneracy in ^{60}Ca and a 2.5 MeV gap in ^{68}Ni (see Fig. 28 in [29]). To assess this gap we compute the spectroscopic strength functions for the $\nu 1g_{9/2}$ and $\nu 2d_{5/2}$ orbitals in ^{69}Ni and generate the fragmentation into physical states. The calculations use the Lanczos structure function method [64] over 30 final states and include up to 12 and 11 particle-hole excitations across $Z = 28$ and $N = 50$ for ^{68}Ni and ^{69}Ni, respectively. The results are listed in Table II, in the column labeled LNPS.

The spectroscopic strength appears to concentrate in two principal components around 2.0 and 2.4 MeV, which together account for approximately 86% of the total strength. The degree of fragmentation appears to be sensitive to the size of the $g_{9/2}$–$d_{5/2}$ neutron gap. When this gap is increased by 500 keV (labeled hereafter LNPS†) the location of the peaks is only slightly affected, but the distribution of the strength is significantly rearranged resulting in an improved agreement with experiment, as shown in Table II. The second peak becomes dominant, consistent with the observed data. A comparison with the experimental values is shown in Fig. 4. A third peak at 2893 keV also appears in the LNSP† calculations, close to an experimental peak observed at 2878 keV. The angular distribution of this state is shown in Fig. 3 together with the calculated distributions for $\ell = 2$ and 4. Owing to the large uncertainties and the uncharacteristic angular distribution, a firm assignment is not possible. Assuming $\ell = 2$ the extracted SF would be $0.12 \pm 0.01^{[+0.14]}_{[-0.02]}$, in good agreement with the LNPS† prediction. This upper limit is shown in Fig. 4. The point at the largest c.m. angle, however, seems to suggest the presence of an $\ell = 4$ component.

The extracted gap has broader implications for the structure of nuclei in this region, particularly within the $N = 40$ island of inversion. The onset of collectivity in this region is driven by the reduced $g_{9/2}$–$d_{5/2}$ spacing, which favors quadrupole correlations in Cr and Fe isotopic chains [33].

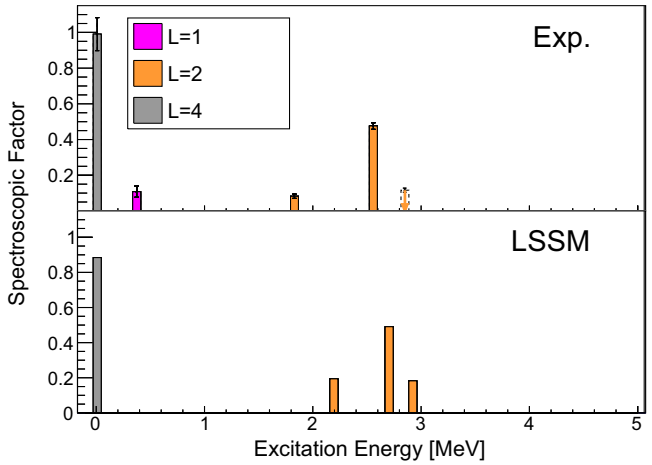

FIG. 4. Comparison between experimental and theoretical spectroscopic factors. Top panel: Experimental spectroscopic factors for states in ^{69}Ni, as shown in Fig. 3, based on the spin-parity assignments listed in Table I. The SF indicated for the 2878 keV state indicates an upper limit obtained by assuming that the state corresponds to a pure $\ell = 2$ transfer. Error bars represent statistical uncertainties; see text for a discussion of systematic contributions. Bottom panel: Spectroscopic factors from large-scale shell-model (LSSM) calculations using the LNPS† effective interaction. $\ell = 1$ states were not included in the calculations. The state at 1768 keV, with the smallest spectroscopic factor, is omitted for clarity.

To keep the same features at mid-proton shell, the +500 keV increase applied to ^{68}Ni in the LNPS† interaction was counterbalanced by a −500 keV shift in ^{60}Ca.

The corresponding evolution of neutron effective single-particle energies is shown in Fig. 5, where an inversion of the $g_{9/2}$ and $d_{5/2}$ orbitals is now clearly observed in ^{60}Ca. The LSSM calculations, with the LNPS† interaction adjusted for the present experimental results, also agree with the inversion predicted by the ab-initio coupled cluster calculations with interactions based on chiral effective field theory [65].

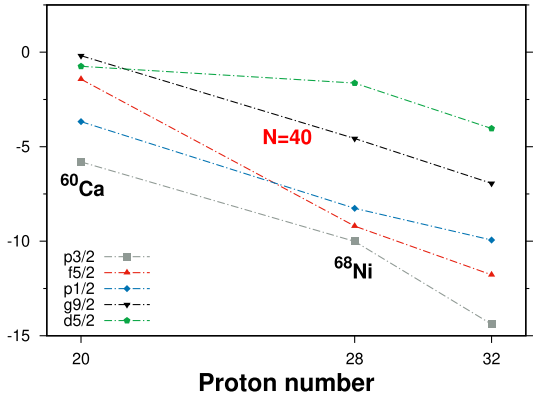

FIG. 5. Neutron effective single particle energies of the LNPS† effective interaction.

In summary, a measurement of the ^{68}Ni(d, p) reaction in inverse kinematics has revealed new excited states in ^{69}Ni, providing critical insight into neutron single-particle structure near $N = 40$. A large spectroscopic factor for the $\ell = 4$ transfer to the ground state confirms the dominance of the $\nu g_{9/2}$ component in that state. A strongly populated state at 2.56 MeV is identified as the principal fragment of the $\nu d_{5/2}$ strength, with additional contributions possibly residing at higher excitation energies. The results are well reproduced by large-scale shell-model calculations with a modified LNPS interaction, indicating a $g_{9/2}$–$d_{5/2}$ spacing of approximately 3 MeV—slightly larger than in lighter Ni isotopes [66–68]. These findings refine our understanding of shell evolution and shape coexistence near $N = 40$, and point to a reordering of single-particle orbitals in ^{60}Ca, where an inversion of the $\nu g_{9/2}$ and $\nu d_{5/2}$ orbitals is predicted near the neutron drip line.

Acknowledgments—A. C. wishes to thank B. R. Jones for providing the detector dead layer measurements and the fruitful discussions about the ISSSort code, and A. M. Moro for useful discussions regarding the DWBA and ADWA calculations. This project has received funding from the European Union's Horizon Europe Research and Innovation programme under Grant Agreement No. 101057511, from the Research Foundation–Flanders under Projects No. I002619N, No. I002919N, and No. I012420N of the International Research Infrastructure program, from the KU Leuven internal funds under Project No. C14/22/104, and from the Science and Technology Facilities Council (UK) Grants No. ST/M00161X/1, No. ST/N002563/1, No. ST/P004598/1, No. ST/V001027/1, No. ST/Y000323/1, No. ST/Y000382/1, and No. ST/Y000242/1. A .H., A. K., M. V. M., and H. T. are grateful for funding from the Knut and Alice Wallenberg Foundation under No. KAW 2020.0076. This work was supported in part by the UK Science and Technology Facilities Council under Grants No. ST/T004797/1 (to D. K. S.) and No. ST/V001116/1 (Manchester).

Data availability—Data and code for this Letter can be found at the KU Leuven Research Data Repository [56,69].

[1] K. Heyde and J. L. Wood, Rev. Mod. Phys. **83**, 1467 (2011).
[2] J. L. Wood and K. Heyde, J. Phys. G **43**, 020402 (2016).
[3] A. N. Andreyev *et al.*, Nature (London) **405**, 430 (2000).
[4] J. Ojala *et al.*, Commun. Phys. **5**, 213 (2022).
[5] B. A. Marsh *et al.*, Nat. Phys. **14**, 1163 (2018).
[6] C. Thibault, R. Klapisch, C. Rigaud, A. M. Poskanzer, R. Prieels, L. Lessard, and W. Reisdorf, Phys. Rev. C **12**, 644 (1975).
[7] G. Huber, F. Touchard, S. Büttgenbach, C. Thibault, R. Klapisch, H. T. Duong, S. Liberman, J. Pinard, J. L. Vialle, P. Juncar, and P. Jacquinot, Phys. Rev. C **18**, 2342 (1978).

[8] C. Détraz, D. Guillemaud, G. Huber, R. Klapisch, M. Langevin, F. Naulin, C. Thibault, L. C. Carraz, and F. Touchard, Phys. Rev. C **19**, 164 (1979).
[9] D. Guillemaud-Mueller, C. Detraz, M. Langevin, F. Naulin, M. de Saint-Simon, C. Thibault, F. Touchard, and M. Epherre, Nucl. Phys. **A426**, 37 (1984).
[10] G. Neyens, M. Kowalska, D. Yordanov, K. Blaum, P. Himpe, P. Lievens, S. Mallion, R. Neugart, N. Vermeulen, Y. Utsuno, and T. Otsuka, Phys. Rev. Lett. **94**, 022501 (2005).
[11] M. Madurga *et al.*, Phys. Rev. C **109**, L061301 (2024).
[12] K. Wimmer *et al.*, Phys. Rev. Lett. **105**, 252501 (2010).
[13] K. Heyde and J. L. Wood, J. Phys. G **17**, 135 (1991).
[14] T. Glasmacher, B. Brown, M. Chromik, P. Cottle, M. Fauerbach, R. Ibbotson, K. Kemper, D. Morrissey, H. Scheit, D. Sklenicka, and M. Steiner, Phys. Lett. B **395**, 163 (1997).
[15] B. Bastin *et al.*, Phys. Rev. Lett. **99**, 022503 (2007).
[16] F. Nowacki and A. Poves, Phys. Rev. C **79**, 014310 (2009).
[17] Y. Utsuno, T. Otsuka, B. A. Brown, M. Honma, T. Mizusaki, and N. Shimizu, Phys. Rev. C **86**, 051301(R) (2012).
[18] M. Bernas, P. Dessagne, M. Langevin, J. Payet, F. Pougheon, and P. Roussel, Phys. Lett. B **113**, 279 (1982).
[19] O. Sorlin *et al.*, Phys. Rev. Lett. **88**, 092501 (2002).
[20] C. Guénaut, G. Audi, D. Beck, K. Blaum, G. Bollen, P. Delahaye, F. Herfurth, A. Kellerbauer, H.-J. Kluge, J. Libert, D. Lunney, S. Schwarz, L. Schweikhard, and C. Yazidjian, Phys. Rev. C **75**, 044303 (2007).
[21] S. Rahaman, J. Hakala, V.-V. Elomaa, T. Eronen, U. Hager, A. Jokinen, A. Kankainen, I. Moore, H. Penttilä, S. Rinta-Antila, J. Rissanen, A. Saastamoinen, C. Weber, and J. Äystö, Eur. Phys. J. A **34**, 5 (2007).
[22] N. Bree *et al.*, Phys. Rev. C **78**, 047301 (2008).
[23] S. Calinescu *et al.*, Phys. Rev. C **104**, 034318 (2021).
[24] W. F. Mueller *et al.*, Phys. Rev. C **61**, 054308 (2000).
[25] F. Flavigny *et al.*, Phys. Rev. C **91**, 034310 (2015).
[26] F. Flavigny *et al.*, Phys. Rev. C **99**, 054332 (2019).
[27] S. Suchyta, S. N. Liddick, Y. Tsunoda, T. Otsuka, M. B. Bennett, A. Chemey, M. Honma, N. Larson, C. J. Prokop, S. J. Quinn, N. Shimizu, A. Simon, A. Spyrou, V. Tripathi, Y. Utsuno, and J. M. VonMoss, Phys. Rev. C **89**, 021301(R) (2014).
[28] B. Crider *et al.*, Phys. Lett. B **763**, 108 (2016).
[29] F. Nowacki, A. Obertelli, and A. Poves, Prog. Part. Nucl. Phys. **120**, 103866 (2021).
[30] C. Santamaria *et al.*, Phys. Rev. Lett. **115**, 192501 (2015).
[31] A. Gade, R. V. F. Janssens, D. Bazin, P. Farris, A. M. Hill, S. M. Lenzi, J. Li, D. Little, B. Longfellow, F. Nowacki, A. Poves, D. Rhodes, J. A. Tostevin, and D. Weisshaar, Phys. Rev. C **103**, 014314 (2021).
[32] M. Cortés *et al.*, Phys. Lett. B **800**, 135071 (2020).
[33] S. M. Lenzi, F. Nowacki, A. Poves, and K. Sieja, Phys. Rev. C **82**, 054301 (2010).
[34] A. Gade *et al.*, Phys. Rev. Lett. **112**, 112503 (2014).
[35] B. Olaizola, L. M. Fraile, H. Mach, A. Poves, A. Aprahamian, J. A. Briz, J. Cal-González, D. Ghiţa, U. Köster, W. Kurcewicz, S. R. Lesher, D. Pauwels, E. Picado, D. Radulov, G. S. Simpson, and J. M. Udías, J. Phys. G **44**, 125103 (2017).
[36] T. Lokotko *et al.*, Phys. Rev. C **101**, 034314 (2020).
[37] J. Ljungvall *et al.*, Phys. Rev. C **81**, 061301(R) (2010).
[38] A. Gade, B. Longfellow, R. Janssens *et al.*, Nat. Phys. **21**, 37 (2025).
[39] M. Rocchini *et al.*, Phys. Rev. Lett. **130**, 122502 (2023).
[40] M. Moukaddam, G. Duchêne, D. Beaumel, J. Burgunder, and L. Caceres, Acta Phys. Pol. B **42**, 541 (2011).
[41] M. Moukaddam, Evolution of the shell structure in medium-mass nuclei: Search for the $2d_{5/2}$ neutron orbital in ^{69}Ni, Ph.D. thesis, Université de Strasbourg, 2012, https://theses.hal.science/tel-00746802.
[42] V. Fedosseev, K. Chrysalidis, T. D. Goodacre, B. Marsh, S. Rothe, C. Seiffert, and K. Wendt, J. Phys. G **44**, 084006 (2017).
[43] Y. Kadi, Y. Blumenfeld, W. V. Delsolaro, M. A. Fraser, M. Huyse, A. P. Koufidou, J. A. Rodriguez, and F. Wenander, J. Phys. G **44**, 084003 (2017).
[44] L. Gaffney *et al.* (s.d.) (to be published).
[45] A. Wuosmaa, J. Schiffer, B. Back, C. Lister, and K. Rehm, Nucl. Instrum. Methods Phys. Res., Sect. A **580**, 1290 (2007).
[46] L. P. Gaffney, D. J. Clarke, H. Johansson, A. Ceulemans, B. Jones, P. MacGregor, and H. T. Törnqvist, Isoldesolenoidalspectrometer/ISSSort: v3.0, 10.5281/zenodo.10694756 (2024).
[47] R. Brun and F. Rademakers, Nucl. Instrum. Methods Phys. Res., Sect. A **389**, 81 (1997).
[48] A. Matta, P. Morfouace, N. de Séréville, F. Flavigny, M. Labiche, and R. Shearman, J. Phys. G **43**, 045113 (2016).
[49] M.Wang, G.Audi, A. H. Wapstra, F. G. Kondev, M.MacCormick, X.Xu, and B.Pfeifferand, Chin. Phys. C **36**, 1603 (2012).
[50] A. Koning and J. Delaroche, Nucl. Phys. **A713**, 231 (2003).
[51] W. W. Daehnick, J. D. Childs, and Z. Vrcelj, Phys. Rev. C **21**, 2253 (1980).
[52] I. J. Thompson, Comput. Phys. Rep. **7**, 167 (1988).
[53] J. A. Tostevin, *University of surrey corrected and updated version of the code* TWOFNR (of M. Toyama, M. Igarashi and N. Kishida) and code FRONT (private communication).
[54] G. Kramer, H. Blok, and L. Lapikás, Nucl. Phys. **A679**, 267 (2001).
[55] B. P. Kay, J. P. Schiffer, and S. J. Freeman, Phys. Rev. Lett. **111**, 042502 (2013).
[56] A. Ceulemans, Code for: the IS587 experiment Ni68(d,p)—transfer, 10.48804/3TF05N (2024).
[57] W. F. Mueller, B. Bruyneel, S. Franchoo, H. Grawe, M. Huyse, U. Köster, K.-L. Kratz, K. Kruglov, Y. Kudryavtsev, B. Pfeiffer, R. Raabe, I. Reusen, P. Thirolf, P. Van Duppen, J. Van Roosbroeck, L. Vermeeren, W. B. Walters, and L. Weissman, Phys. Rev. Lett. **83**, 3613 (1999).
[58] C. Nesaraja, Nucl. Data Sheets **115**, 1 (2014).
[59] R. Grzywacz *et al.*, Phys. Rev. Lett. **81**, 766 (1998).
[60] J. I. Prisciandaro, P. F. Mantica, A. M. Oros-Peusquens, D. W. Anthony, M. Huhta, P. A. Lofy, and R. M. Ronningen, Phys. Rev. C **60**, 054307 (1999).
[61] J. P. Schiffer, C. R. Hoffman, B. P. Kay, J. A. Clark, C. M. Deibel, S. J. Freeman, M. Honma, A. M. Howard, A. J. Mitchell, T. Otsuka, P. D. Parker, D. K. Sharp, and J. S. Thomas, Phys. Rev. C **87**, 034306 (2013).
[62] A. P. Zuker, J. Retamosa, A. Poves, and E. Caurier, Phys. Rev. C **52**, R1741 (1995).

[63] A. P. Zuker, A. Poves, F. Nowacki, and S. M. Lenzi, Phys. Rev. C **92**, 024320 (2015).
[64] E. Caurier, G. Martínez-Pinedo, F. Nowacki, A. Poves, and A. P. Zuker, Rev. Mod. Phys. **77**, 427 (2005).
[65] G. Hagen, M. Hjorth-Jensen, G. R. Jansen, R. Machleidt, and T. Papenbrock, Phys. Rev. Lett. **109**, 032502 (2012).
[66] R. H. Fulmer, A. L. McCarthy, B. L. Cohen, and R. Middleton, Phys. Rev. **133**, B955 (1964).
[67] T. Anfinsen, K. Bjørndal, A. Graue, J. Lien, G. Sandvik, L. Tveita, K. Ytterstad, and E. Cosman, Nucl. Phys. **A157**, 561 (1970).
[68] J. Diriken *et al.*, Phys. Rev. C **91**, 054321 (2015).
[69] A. Ceulemans *et al.* (ISS Collaboration), Data for: The IS587 experiment Ni68(d,p)—transfer, 10.48804/ACXORT (2024).